arXiv:submit/4020126 [cond-mat.mtrl-sci] 9 Nov 2021

Effect of substitutional doping and disorder on the phase stability, magnetism, and half-metallicity of Heusler alloys

N.A. Zarkevich[a], P. Singh[a], A.V. Smirnov[a], Duane D. Johnson[a,c]

[a]*Ames Laboratory, U.S. Department of Energy, Iowa State University, Ames, Iowa 50011 USA*

[b]*Materials Science & Engineering, Iowa State University, Ames, Iowa 50011 USA*

Abstract

Spintronics is the fast growing field that will play a key role in optimizing power consumption, memory, and processing capabilities of nanoelectronic devices. Heusler alloys are potential candidates for application in spintronics due to their room temperature (RT) half-metallicity, high Curie temperature, low lattice mismatch with most substrates, and strong control on electronic density of states at Fermi level. In this work, we investigate the effect of substitutional doping and disorder on the half-metallicity, phase stability, and magnetism of Heusler alloys using density functional theory methods. Our study shows that electronic and magnetic properties of half/full-Heusler alloys can be tuned by changing electron-count through controlled variation of chemical compositions of alloying elements. We provide a detailed discussion on the effect of substitutional doping and disorder on the tunability of half-metallic nature of Co_2MnX and NiMnX based Heusler alloys, where X represents group 13–16 and period 3–6 elements of the periodic table. Based on the idea of electron count and disorder, we predicted a possible existence of thermodynamically stable half-metallic multicomponent bismuthides, for example, $(CuNi_3)Mn_4Bi_4$ and $(ZnNi_7)Mn_8Bi_8$, through substitution doping at Ni site by specific Cu and Zn composition in half-Heusler NiMnBi. We believe that the design guide based on electron-counts presented for half-metals will play a key role in electronic-structure engineering of novel Heusler alloys for spintronic application, which will accelerate the development and synthesis of novel materials.

Keywords: Spintronics, Heusler, Half-metal, Density-functional theory, materials discovery

1. Introduction

Heusler alloys [1] are a large class of naturally occurring [2] and manufactured [3] ternary intermetallic compounds with $L2_1$ full Heusler (fH) or $C1_b$ half-Heusler (hH) structure (sometimes called semi-Heusler), which can be partially disordered [4–10]. Many Heuslers are ferromagnetic (FM), with Curie temperatures T_c between 200 and 1100 K [11–13]. The ones with T_c near room temperature were considered for magnetocalorics [14, 15]. Some alloys have a band gap in the minority spins, which may (as in half-metals [16–23]) or may not be at the Fermi energy. A half-metal conducts electrons with one spin orientation, but acts as an insulator or a semiconductor (with a band gap at the Fermi energy E_F) to those with the opposite spins. Half-metals are used in small-scale magnetic and spin filtering devices and switches [24], and find applications in magnetic materials [25]. The band-gap engineering [26, 27] helps to create materials for advanced electronic devices. Such solid-state devices are used in spintronics – a rapidly developing branch of electronics, incorporating electron spin degree of freedom [28, 29]. Materials discovery can be greatly accelerated by theoretical guidance [14, 30–33], in particular, electronic-structure engineering of doped and chemically disordered alloys. However, there has been scant attention on disorder based Heusler alloys. Composition tuning, i.e., disorder, in these alloys can modify the Fermi level E_F, and alter the electronic, magnetic, and other physical properties [23, 34–36].

*Corresponding authors email:psingh84@ameslab.gov

[1]NAZ and PS equally contributed to this work.

Here, we study the electronic structure and its dependence on composition in fully and partially ordered Heusler alloys using density-functional theory (DFT) methods, some of which are half-metallic. The electronic properties of the doped fH M_2MnX and hH MMnX alloys with M={Co, Ni} and X={Al, Ga, In, Tl; Si, Ge, Sn, Pb; P, As, Sb, Bi; S, Se, Te}, elements from groups 13–16 and periods 3–6 in the Mendeleev Periodic Table were analyzed in detail. We also mix Mn with Fe in $Co_2(Mn_{1-x}Fe_x)A$, where A is Sn or Sb, and $0 \le x \le 1$. We show that in fH Co_2MnX alloys, the width of the minority-spin band gap E_{gap} decreases along the period (3–6) and increases along the group (13–16) of X.

We found that the electronic structure analysis of fH Co_2MnX and hH NiMnX shows compositional interval for half-metals in terms of the *electron count* (n). The considered hH NiMnX alloys show a energy gap in the minority spins at (band-gap) or slightly above (pseudo-gap) the Fermi level. Five of them (with X=Si, Ge; P, As, Sb) could be half-metals, but only one (NiMnSb) was found stable. The structural stability restricts design of hH half-metals. Based on electron count per atom analysis, we predicted a possible existence of weakly stable half-metallic multicomponent bismuthides. Half-metals often have lower formation energies (and hence are more stable) than metals. Considering a doped hH NiMnBi, we found that adding from 0.3 to 1.3 electrons per formula unit (e^-/f.u.) would turn this compound into a half-metal; we confirm this prediction for the quaternary $CuNi_3Mn_4Bi_4$ and $ZnNi_7Mn_8Bi_8$ alloys. The stability of Heusler alloys was analyzed by considering relative structural energies and cross-sections of the ground-state hull. The phase stability analysis suggests that most of these alloys are energetically stable. Small formation enthalpies calculated from DFT methods indicates the preference of the stable alloys for substitutional disordering. Our results provide a valuable guidance for adjustment of the width and position of the band gap in the minority spins relative to the Fermi energy E_F.

2. Computational Methods

2.1. Density-functional theory methods

Vienna Ab-initio Simulation Package (VASP): We used VASP [37, 38] with the projector augmented waves (PAW) [39, 40] and Perdew, Burke and Ernzerhof revised for solids (PBEsol) exchange-correlation functional [41]. We used a dense Γ-centered mesh [42] with at least 72 k-points per Å^{-1} for the Brillouin zone integration. The tetrahedron method with Blöchl corrections [43] was used to calculate electronic density of states (DOS), while Gaussian smearing with $\sigma = 0.05$ eV was used within the conjugate gradient algorithm for the full structural relaxation at zero pressure. We calculated the structural energies, using either primitive unit cells for ternary line compounds, or supercells for the multicomponent alloys. For example, $CuNi_3Mn_4Bi_4$ was considered in a 12-atom conventional cubic unit cell of the hH structure, while $ZnNi_7Mn_8Bi_8$ was addressed in a 24-atom $6.141 \times 6.141 \times 12.305$ Å supercell using $12 \times 12 \times 6$ k-point mesh. $Co_2Mn_1(Sn_nSb_{1-n})$ alloys were considered using a decorated 16-atom conventional cubic unit cell of the fH structure, shown in Fig. 1a. The phonon calculations were performed using supercell (96 atoms) of the conventional NiMnBi $C1b$ unit cell (12 atoms), and finite displacement approach with atomic displacement distance of 0.01 Å [90].

Korringa-Kohn-Rostoker coherent potential approximation (KKR-CPA): Green's function based KKR-CPA method [44, 45][46] is suitable for both fully ordered and partially disordered multicomponent systems. It treats multiple scattering in the atomic spheres approximation (ASA) [47]. We use the optimal local basis set [46] with the radii of scattering spheres, determined from the atomic charge distributions around each atom and its neighbors. The periodic boundary correction takes into account both electrostatic energy [48] and Coulomb potential. Use of the variational definition [49] of the muffin-tin potential zero v_0 and a proper representation of the topology of charge density in the optimal basis set allows to approach accuracy of the full-potential methods [50].

Our truncated optimal basis set with $l_{\max}$=3 includes s-, p-, d- and f-orbitals; we find a negligible sensitivity of energy differences to the higher-order spherical harmonics. Integration in a complex energy plane uses the Chebyshev quadrature semicircular contour with 20 points. The Brillouin zone integration is performed using a special k-points method [42] with a 12×12×12 mesh for disordered or ordered systems with 4 atoms per unit cell and 8×8×8 (6×6×6) mesh for ordered systems with 16 atoms/cell. We use the Perdew, Burke and Ernzerhof revised for solids (PBEsol) [41]. Self-consistency in spin-polarized calculations were was achieved using the modified Broyden's second method [51]. The homogeneous substitutional chemical disorder is considered using the coherent potential approximation (CPA) [52] with the mean-field corrections [53].

Tight-binding-Linearized Muffin-tin Orbital Method: We use the van Leeuwen-Baerends corrected LDA exchange (LDA+vLB) [54–60] with the exchange-correlation energy parameterization [61]. An improved ASA basis of TB-LMTO [62] includes atomic spheres and empty spheres (ESs). The sum of the volumes of all the spheres is equal the total volume of the periodic unit cell. The radii of the spheres are chosen to have their overlaps close to the local maxima or saddle points of the electrostatic potential. The positions of the ES centers are at the high-symmetry points between atoms. The relaxed atomic positions are taken from VASP output. ESs are treated as empty sites with no cores and small electronic charge density. Because the contribution of exchange in empty spheres is very small, the vLB-correction is calculated only in the atomic spheres [54–59, 63–65].

Self-consistently was achieved when the change of charge density and energy is below 10^{-5} and $< 10^{-4}$ Ry/atom, respectively [62]. The k-space integration is done using the tetrahedron method with the $12 \times 12 \times 12$ mesh. In theory, the Coulomb and exchange self-interactions should be cancelled [57–59]. The LDA and GGA are known to under-estimate band gaps; this problem is less severe in GGA due to the gradient correction [66]. On the other hand, the asymptotic vLB correction significantly improves the exchange potential both near the nucleus ($r \to 0$) and at the large-distance limit ($1/r \to 0$). It correctly describes the valence and conduction-band energies, and provides the band gaps comparable to those measured in experiments [57–59].

2.2. Energy-gap estimate

The width of the band gap is estimated from the plateau in the total number of the minority-spin electrons $n_s(E)$ (more detail in Fig. 4c). Counting electrons in the majority-spin channel, we find the number of electrons n_- (n_+) that should be added [$n > 0$] or removed [$n < 0$] to move the highest occupied band (the lowest unoccupied band) in the minority spins to the Fermi level. These numbers define the compositional interval of half-metallicity in terms of the electron count.

3. Results and discussion

Crystal Structure: The full-Heusler and half-Heusler ternary alloys, shown in Fig. 1a, crystallize in $L2_1$ and $C1_b$ structures, respectively. The fH M_2ZX structure ($L2_1$, cF16, with Cu_2MnAl prototype, $Fm\bar{3}m$ cubic space group #225) has a cubic conventional unit cell with 16 sites of 3 types, which consists of four interpenetrating fcc sublattices with positions (0,0,0) and $(\frac{1}{2},\frac{1}{2},\frac{1}{2})$ for M, $(\frac{1}{4},\frac{1}{4},\frac{1}{4})$ for Z (Mn) and $(\frac{3}{4},\frac{3}{4},\frac{3}{4})$ for X atoms. The primitive unit cell has only 4 sites. The atoms decorate a body centered cubic (bcc) lattice. The hH M_1ZX structure ($C1_b$, cF12, with MgAgAs prototype, $F\bar{4}3m$ space group #216) differs from cF16 fH by a vacancy on $(\frac{1}{2},\frac{1}{2},\frac{1}{2})$ sites.

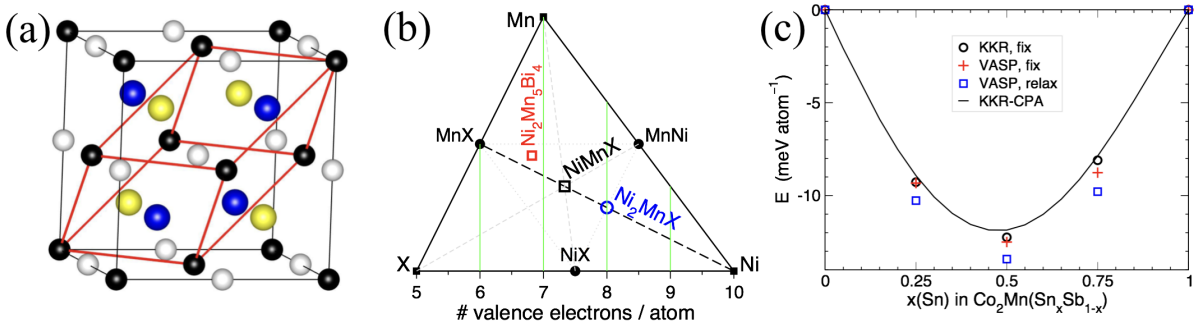

Figure 1: (a) The quaternary Heusler LiMgPdSn-type cubic structure with $F\bar{4}3m$ space symmetry group (#216) has atoms on the bcc cites. The $C1_b$, cF12 ($F\bar{4}3m$, #216) hH AgAsMg-type MMnX differs from the $L2_1$, cF16 ($Fm\bar{3}m$, #225) fH Cu_2MnAl-type M_2MnX structure by vacancies on $(\frac{1}{2},\frac{1}{2},\frac{1}{2})$ sites (white). M is black (black and white in fH), Mn is blue, and X is yellow. The conventional (cubic) and primitive unit cells are shown by black and red lines, respectively. (b) Ternary phase diagram with iso-surfaces of electron count per atom (vertical green lines) for Ni-Mn-X alloys with group 15 elements X = {P, As, Sb, Bi}. (c) Mixing enthalpies (meV/atom) of $Co_2Mn_1(Sn_xSb_{1-x})$ at 0 K (DFT).

Substitutional elements: We consider M_2ZX fH and M_1ZX hH alloys with M={Co, Ni}; Z={Mn}; and X={Al, Ga, In, Tl; Si, Ge, Sn, Pb; P, As, Sb, Bi; S, Se, Te}, as well as mixed $Co_2(Mn_{1-x}Fe_x)A$ with A={Sn or Sb}. Our investigation covers both fully ordered and partially disordered (substitutionally doped) alloys.

Electron count and composition: Historically, the search for half-metals started from line compounds [67]. We emphasize that the Fermi level E_F remains in the band gap within a range of energies, bounded by the highest occupied and the lowest unoccupied states in the minority spins, and there is a corresponding range of half-metallic compositions. Indeed, the number of valence electrons $N(c)$ depends on elemental composition c. Fig. 1b illustrates the inverse, many-to-one $c(N)$ relation for the ternary Ni-Mn-X alloys. Thus, a fixed N specifies a set of compositions, leaving a sufficient freedom in choosing chemical elements for doping. For example, hH alloys with compositions $NiMn(P_xAs_ySb_zBi_w)$, where $0 \le \{x, y, z, w\} \le 1$ and $x + y + z + w = 1$, have $N = 7\frac{1}{3}$, see Fig. 1b. Below we express the electron count n as a difference in the number of valence electrons relative to a line compound.
Half-metallic range: In each compound, we find a band gap in the minority spins (if any) of the width $E_{gap} = (E_+ - E_-)$ at the electronic energies E in the range $E_- \le (E - E_F) \le E_+$. A compound is half-metallic, if the Fermi level happens to be in this gap (thus, $E_- < 0$ and $E_+ > 0$).

The number of electronic states at energies below E_0 is

$$N(E_0) = \int_{-\infty}^{E_0} g(E)dE, \tag{1}$$

where g is the electronic density of states (DOS) for both spins. At zero electronic temperature, all states below the Fermi energy E_F are filled, hence $N(E_F)$ is equal to the total number of electrons N. (If one uses pseudopotentials or does not count core electrons, then one can use the total number of valence electrons.) A band gap in the minority spins covers a ragne of both occupied and empty electronic states from $N_- \equiv N(E_F + E_-)$ to $N_+ \equiv N(E_F + E_+)$; those are the edges of the band gap. Next, we use eq. 1 to find the differences

$$n_\pm \equiv (N_\pm - N) = \int_{E_F}^{E_F + E_\pm} g(E)dE. \tag{2}$$

The signs of $E_\pm$ and $n_\pm$ coincide, because $g \ge 0$. A compound is half-metallic, if $n_- < 0$ and $n_+ > 0$, see Table 1 & 2.

Table 1: The minority-spin band gap width E_{gap} (eV) and position in terms of energies $E_\pm$ (relative to E_F) and electron count $n_\pm$ in full-Heusler Co_2MnX ternary line compounds. The unstable compounds are marked with an asterisk (*).

X	n_-	n_+	E_-	E_+	E_{gap}^{GGA}	E_{gap}^{vLB}
	(e/f.u.)		(eV)		(eV)	
Al	0.07	0.84	0.06	0.62	0.56	0.38
Ga	0.5	0.84	0.24	0.55	0.31	0.23
In*	0.9	1.0	0.54	0.64	0.10	–
Tl*	1.1	1.1	0.63	0.63	0.0	0.0
Si	-0.6	0.35	-0.39	0.34	0.73	0.49
Ge	-0.2	0.4	-0.12	0.38	0.50	0.37
Sn	0.1	0.45	0.09	0.44	0.35	0.37
Pb*	0.35	0.5	0.28	0.43	0.15	0.11
P*	-1.1	0.05	-0.76	0.04	0.80	0.55
As*	-0.6	0.05	-0.43	0.05	0.48	0.44
Sb	-0.5	0.03	-0.51	0.02	0.53	0.38
Bi*	-0.1	0.2	-0.08	0.27	0.35	0.26

Within the frozen-band approximation, let us increase the total number of electrons from N to $(N + n)$, where negative n stands for subtracting electrons. The added or subtracted electrons will shift E_F to the band gap (thus making the system half-metallic), if $n_- \le n \le n_+$. In general, doping a conductor with electronic donors or acceptors changes the number of electrons, shifts the Fermi level, and adds impurity states. If those impurity states are not in the band gap, then half-metallicity of the doped system is approximated by inequality ($n_- \le n \le n_+$). Lattice relaxations around impurities and defects broaden the bands and narrow the band gap. In addition, sometimes electronic bands of the dopant can appear in the band gap. These effects narrow both the band gap and the half-metallic compositional range. With this caution, inequality ($n_- \le n \le n_+$) and Tables 1 and 2 provide a practical guidance for engineering of the half-metallic Heusler alloys.

Table 2: The minority-spin band gap E_{gap} and its position in terms of energies $E_{\pm}$ and electron count $n_{\pm}$ in half-Heusler NiMnX compounds.

X	n_-	n_+	E_-	E_+	E_{gap}^{GGA}	E_{gap}^{vLB}
	(e/f.u.)		(eV)		(eV)	
Al*	0.6	1.2	0.10	0.90	0.80	–
Ga*	0.9	1.3	0.30	1.00	0.70	–
In*	1.25	1.5	0.46	0.88	0.40	0.32
Tl*	1.4	1.6	0.60	0.90	0.30	0.27
Si*	-0.37	0.45	-0.35	0.56	0.91	0.8
Ge*	-0.0	0.57	-0.0	0.7	0.70	0.6
Sn*	0.40	0.72	0.28	0.74	0.46	0.43
Pb*	0.65	0.87	0.45	0.79	0.34	0.28
P*	-0.67	0.22	-0.66	0.28	0.93	0.7
As*	-0.37	0.30	-0.38	0.39	0.77	0.6
Sb	-0.17	0.22	-0.27	0.28	0.55	0.45
Bi*	0.06	0.31	0.07	0.47	0.40	0.34

Known half-metals among ternary systems include full Heusler Co_2MnX with X={Si, Ge, Sb} and half-Heusler NiMnSb compounds, which is in agreement with the findings of Ma *et al.* [68]. We also emphasize that not only the line compounds, but also ranges of compositions (with off-stoichiometric disorder) can be half-metallic. We compute the compositional ranges, which keep known half-metals half-metallic, and predict the level of doping, which can turn others (like Co_2MnSn and hypothetical NiMnBi) into half-metals. Table 2 can be used to design half-metals of composition $(Ni_{1-z-y}Cu_zZn_y)MnX$ with X={Al, Ga, In, Tl; Si, Ge, Sn, Pb; P, As, Sb, Bi}. For each X, we predicted a range of $n = (z + 2y)$, at which this doped half-Heusler alloy is half-metallic. For negative n, Ni can be mixed with Co and Fe to make $(Ni_{1-z-y}Co_zFe_y)MnX$ alloys, where $(z + 2y) = |n| > 0$. Dopants narrow the band gap, hence the actual composition range could be narrower than that predicted from electron count.

Phase stability – formation energy of Co-Mn-Sn-Sb Heusler alloys: We show DFT calculated mixing enthalpies (E_{mix}) of $Co_2Mn_1(Sn_xSb_{1-x})$ with fixed direct atomic coordinates (fix) in Fig. 1c, and compared those with fully relaxed atoms (relax). The ordered structures with 16-atom cells are addressed by VASP and KKR. On the other hand, the disorder on the Sn/Sb sublattice was modeled in the 4-atom primitive cell (shown in Fig. 1a), and E_{mix} was calculated using KKR-CPA. The E_{mix} shows the stability for each structure on the ground-state (GS) hull in Fig. 1c. The structures with energies above the GS hull are either unstable or metastable, which might be stabilized by entropy at finite temperature. Our calculations show good agreement for predicted E_{mix} across the DFT methods, which emphasizes the accuracy of DFT calculations.

To avoid a systematic error in the energy of α-Mn, resulting from application of DFT to an astonishingly complex α-Mn crystal structure with non-collinear moments, we use the semi-empirical energy of metallic Mn, obtained from the calculated energies of metallic Bi [36] and ferrimagnetic MnBi (with NiAs structure) [69], and the experimental [70] E_{mix} of MnBi of -0.204 eV/f.u. By construction, the calculated formation energy of MnBi coincides with this experimental value.

Electronic-structure engineering: We compare the calculated electronic DOS for the ternary line compounds Co_2MnX and Ni_1MnX in Fig. 2. We use experimental data to mark the known stable compounds. Our values of $E_{\pm}$ and $n_{\pm}$, defined in section IIIA, are provided in Tables I and II for fH-Co_2MnX and hH-NiMnX (which have the minority-spin band gap in the vicinity of E_F). This data is useful for engineering materials with a modified electronic structure and for predicting the band gaps in disordered alloys, some of which will be considered in section IV B.

In Fig. 2a,b, we plot total spin DOS (states/eV·f.u.) for (a) fH Co_2MnX, and (b) hH NiMnX alloys. Quite interestingly, we found energy gap or pseudo-gaps in the minority-spin near/at E_F for both stable and unstable ferromagnetic compounds. In fH Co_2MnX the gaps are at or near E_F. Similarly, in hH NiMnX they are at or slightly above E_F. In contrast, there are no half-metals among fH Ni_2MnX alloys (see Fig. S1). Because Ni has more electrons than Co, the difference between the fH Co_2MnX and Ni_2MnX is expected from the electron count, as shown in Table 1 & 2. Indeed, the gaps are near E_F in Co_2MnX, but quite far (~ 1 eV) below E_F in Ni_2MnX.

Tables 1 and 2 show the band gap $E_{gap} = (E_+ - E_-)$ for the minority spins from GGA (VASP) and LDA+vLB [72]

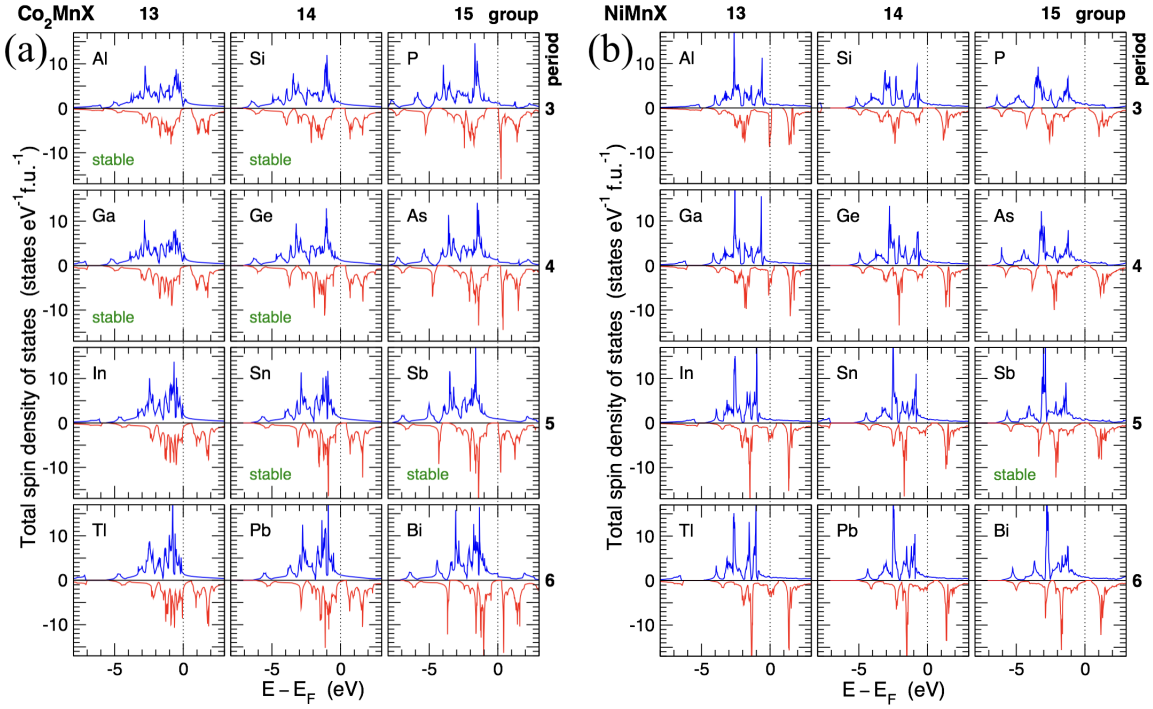

Figure 2: Total spin DOS (states/eV·f.u.) of the (a) fH Co_2MnX, and (b) hH NiMnX alloys for 12 elements X (group 13-15, period 3-6). Stable compounds are known from experiment [11, 12, 71].

calculations. The gap extends from E_- to E_+ (both energies are relative to E_F); for half-metals, these are energies of the highest occupied and the lowest unoccupied bands in the minority spins. The line compound was categorized half-metallic, if $E_- \leq 0$ and $E_+ \geq 0$ (consequently, $n_- \leq 0$ and $n_+ \geq 0$). For half-metals with off-stoichiometric disorder, the level of doping in terms of n (added electrons per formula unit) lies within the range $[n_-, n_+]$. As explained in section 3, dopants narrow the gap, hence the actual compositional range can be narrower.

The LDA/GGA functionals usually underestimate the band gap in semiconductors and half-metals. This systematic error narrows the predicted compositional range for half-metals. An error in the predicted band gaps is larger in LDA, smaller in GGA [66], and is expected to cancel for the exact exchange and correlation. The LDA+vLB used in this work is a semi-local approximation for the exact exchange that was found to provide quite accurate predictions of semiconductor band-gaps [57]. The LDA correlation with modified LDA+vLB (exact) exchange was used as shown in Tables 1 and 2.

3.1. Alloys with substitutional atomic disorder and comparison with experiments

In materials engineering, consideration of multicomponent alloys with a partial atomic disorder can be challenging. We analyze quantitatively the selected fH alloys in section 3.4. A fH alloy has three sublattices (Fig. 1a). A substitutional doping is possible on each sublattice. In section 3.4, we consider several mixed fH alloys (with disorder on one of the sublattices) and validate predictions, based on the electron count.

Addressing the ternary line compounds, we fully relaxed each structure. We found a reasonable agreement between the calculated and measured [11, 12] lattice constants a and magnetic moments M, see Tables S1 and Table S2. We considered both ferromagnetic (FM) and antiferromagnetic (AFM) spin ordering. For the Co_2MnX systems in Fig. 2, we find that FM ordering is preferred, in agreement with the previous calculations [73]. The calculated [37, 38] magnetization M of Co_2MnSn is 5.03 (5.04) μ_B per formula unit with Sn d-electrons in the core (valence) at the equilibrium lattice constant $a_0 = 5.9854$ Å. It reasonably agrees with the experimental [74] M of 5.08 μ_B. Earlier full-potential FLAPW [75] and our current KKR calculations provide 5.0 μ_B/f.u. at $a_0 = 5.964$ Å and 4.98 μ_B/f.u. at $a_0 = 5.995$ Å, respectively. However, there is an experimental uncertainty in the weight of the powder sample, only a

fraction of which is the desired phase [11]. The imprecisely measured magnetization of the Co_2MnSn and Co_2MnSb polycrystalline powder samples [11] is below the expected theoretical value, which must be integer for a half-metal, and Co_2MnSb was found a half-metal in experiments [11].

3.2. NiMnX half-Heusler alloys

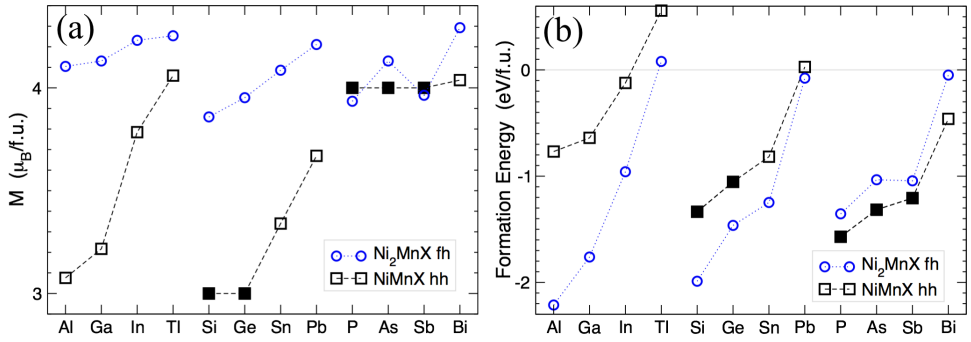

Figure 3: (a) Calculated magnetization (Bohr magnetons per formula unit) for hH NiMnX (black squares). Half-metals are solid symbols. The fH Ni_2MnX (blue circles) are ferrimagnetic in nature (see fH detail in supplement).(b) Formation energy (electron-volts per formula unit) of the hH NiMnX (black squares). Half-metals are solid symbols. We provide formation energy of fH Ni_2MnX alloys (blue circles) for comparison (see fH detail in supplement).

Among the hH NiMnX alloys, where X is one of {Al, Ga, In, Tl; Si, Ge, Sn, Pb; P, As, Sb, Bi}, NiMnSb is the only known stable ternary compound, which had been claimed to be a half-metal [16, 76], but its half-metallicity was questioned by some measurements [77] and calculations [78]. We calculate magnetization (Fig. 3a), formation energy (Fig. 3b), and electronic DOS (Fig. 2 and Fig. S1) of fH Ni_2MnX and hH NiMnX alloys. Magnetization of the half-metallic hH alloys increases from 3 μ_B/f.u. for NiMnSi and NiMnGe containing group 14 elements to 4 μ_B/f.u. in group 15. An anti-ferromagnetic (AFM) spin ordering was found preferable for most compounds of sulfur, a group 16 element with a small atomic size and high electronegativity.

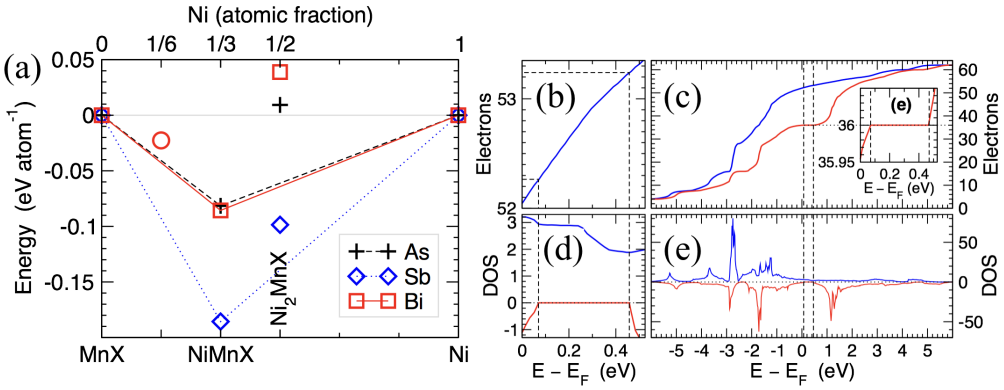

Figure 4: (a) Energy (eV/atom) of the hH NiMnX compounds relative to that of metallic fcc Ni and MnX (X = As, Sb, Bi), see Fig. 1b. Red circle is the energy of the phase-segregated $Ni_2Mn_5Bi_4$ and metallic Bi. Lines are cross-sections of the ground-state hull. (b-d) Number of electrons (per unit cell) and DOS (states/eV cell) of the hH NiMnBi alloy

Among the hH alloys, we found five half-metals: they are NiMnX with X={Si, Ge, P, As, Sb}. The first two with a group 14 element (NiMnSi, NiMnGe) have magnetization of 3 μ_B/f.u., which increases to 4 μ_B/f.u. for the last three (NiMnP, NiMnAs, NiMnSb) with X from group 15. In spite of having large magnetic moments, cubic systems can not make hard magnets due to absence of anisotropy; a structural anisotropy is necessary for a magnetic anisotropy in a hard magnet. All considered hH NiMnX alloys have a gap in the minority spins at or slightly above the Fermi

level (Fig. 2 and Table 1). In general, a peak with a maximum in electronic DOS at the E_F destabilizes the alloy. Electron (or hole) doping is one option, which can help in shifting E_F away from this peak, thus reducing $g(E_F)$. Half-metals are the most stable compounds among the considered hH alloys (Fig. 3b). Fig. 4a shows relative energies of the line compounds. The fH Ni_2MnX alloys with X={As, Bi} are not stable, because their energies are well above the ground-state hull. Although the fH Ni_2MnSb could be stabilized by entropy at finite temperature T, we predict that at low T it tends to segregate towards $Ni_{2-\delta}MnSb$ and metallic Ni, although diffusion is limited at low T. The hH NiMnSb is known to be stable in experiment, and Fig. 4a does not question its stability.

NiMnBi is only 0.06 e^-/f.u. away from being a half-metal; it has a gap in the minority spin channel above the E_F (Fig. 4b-d), and might be turned into a half-metal by electron doping, such as a partial substitution of Ni by Cu or Zn in Fig. 5. From the estimate of the needed level of doping (see Fig. 4b-d and Table 1), we predict that $CuNi_3Mn_4Bi_4$ and $ZnNi_7Mn_8Bi_8$ should be half-metals. The total DOS plot for hH NiMnBi compared to for fH Ni_2MnBi in Fig. 5 shows an opening in the energy-gap in the minority spin, however, some electronic states are still present at the E_F. To fill those electronic states at E_F, we electron doped Ni by adding Cu (0.25)/Zn(0.125). Our supercell calculations show a clear band-gap in the minority spins, although doping narrowed the band gap (see Table 2).

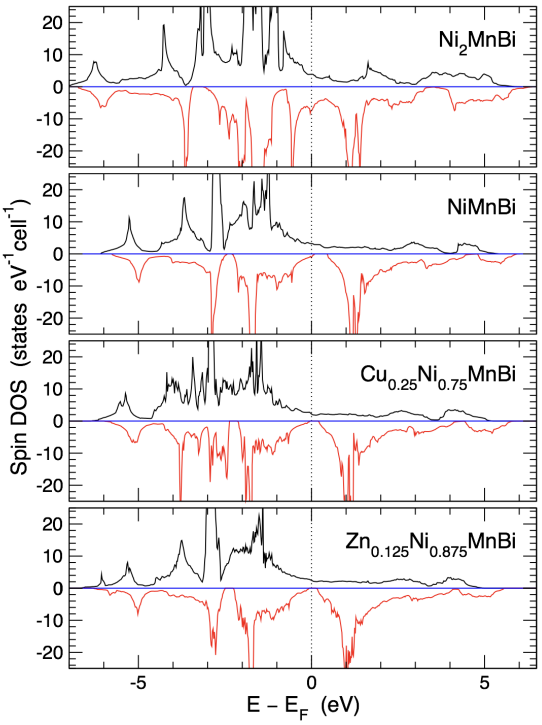

Figure 5: Total spin DOS (states/eV-f.u.) of the fH Ni_2MnBi (unstable), hH NiMnBi, and doped hH alloys with partially substituted Ni. Doping shifts the Fermi level and narrows the band gap in the minority spins.

Half-metals, in general, are thermodynamically more stable than other metallic half-Heuslers as shown in Fig. 3b. We want to emphasize that a negative formation energy (Fig. 3b) relative to the elemental ground states does not necessarily indicate stability of a given phase, because there could be other (more stable) phases nearby, such as the weakly stable $Ni_2Mn_5Bi_4$, NiBi and MnBi in Ni-Mn-Bi system (see Fig. 1b and Table S3). Energies of all possible competing structures are needed for constructing the complete ground-state hull. While an alloy with a negative formation energy might be stable, a positive energy relative to any set of phases indicates that a structure is above the ground-state hull and is definitely unstable towards segregation at low T. However, some of the metastable structures are technologically feasible, especially if the phase transformation or segregation has high enthalpy barriers or a metastable phase is thermally stabilized by entropy; examples are iron steels [79–81], Alnico magnets [82], titanium alloys [83], shape memory alloys [84–86], and graphite [87]. The ferrimagnetic hexagonal MnBi, NiBi, and

magnetic cubic $Ni_2Mn_5Bi_4$ are weakly stable compounds. In particular, determined from the measured heat of combustion [70] formation enthalpy of MnBi is only -4.7 ± 0.1 kcal/g-formula (-0.102 ± 0.002 eV/atom). The measured formation enthalpy of NiBi is approximately -0.93 kcal/g-formula (-0.020 eV/atom); this value was inaccurate due to inhomogeneity of the sample [88]. The calculated formation enthalpies of NiBi and $Ni_2Mn_5Bi_4$ reasonably agree with experiment (Table S3). We also estimated the Curie temperature ($T_c = \frac{2}{3}\frac{\Delta E_{AFM-FM}}{3k_B}$) NiMnBi, $CuNi_3Mn_4Bi_4$, and $ZnNi_7Mn_8Bi_8$, which is higher than room-temperature, i.e., 312 K, 324 K, and 310 K, respectively. The above room-temperature T_c indicates the possible applicability of half-Heusler compounds in spintronic devices. The prediction of dynamical stability [89] is critical for experimentalists to know if compound can be synthesized. Therefore, we carried out phonon calculations [90] of one of the compound, i.e., NiMnBi see Fig. S3, which shows no imaginary phonon modes. This suggests that the predicted compound is both thermodynamically and dynamically stable, which further establishes the quality of our prediction.

Table 3: For selected compounds, $[n_-, n_+]$ range (e^-/f.u.), E_-, E_+, and $E_{gap} = E_+ - E_-$ (eV), and Curie temperature (K) from the supercell calculations, see Table 1 caption.

	n_-	n_+	E_-	E_+	E_{gap}^{GGA}	E_{gap}^{vLB}	T_c
NiMnBi	0.06	0.31	0.07	0.47	0.40	0.34	312
$CuNi_3Mn_4Bi_4$	-0.57	1.1	-0.10	0.25	0.35	0.25	324
$ZnNi_7Mn_8Bi_8$	-0.12	0.2	-0.11	0.19	0.30	—	310

3.3. Effect of spin-orbit coupling on the electron count descriptors

We also provide some discussion on the effect of spin-orbit coupling (SOC) on hh compounds NiMnBi and $CuNi_3Mn_4Bi_4$ to show the efficacy of our predictions. The inclusion of SOC and comparing those with spin-polarized (collinear) calculations suggests that magnetic-moment of both the hh compounds remains quenched [91–94] as we did not notice any significant change in cell or atomic moments. The collinear and SOC moments of NiMnBi and $CuNi_3Mn_4Bi_4$ are (16.09, 16.09) μ_B and (17.00, 17.00) μ_B, respectively. Similar reports on Bi based hh compounds were found [95], where a non-vanishing DOS may appear in the minority gap by the effect of SOC but not major changes appear in electronic-structure that can impact the overall conclusion. Importantly, we also did not notice any significant change in electronic-structure or magnetic behavior arising from SOC, which indicate towards the robustness of our predictions of half-metallic nature in Table 3 [94].

3.4. Partially disordered alloys

The partial disorder in $Co_2Mn(Sn_xSb_{1-x})$, $(Co_xNi_{1-x})_2MnA$ and $Co_2(Mn_{1-x}Fe_x)A$ (here, A={Sn or Sb}) was considered for structural (lattice constant), mixing enthalpy, and electronic-structure in Fig. 6. We emphasize that disorder on different sublattices can produce a similar shift of the E_F. Indeed, the expected similarity of the electronic structure was found between $Co_2Mn(Sn_xSb_{1-x})$ and $Co_2(Mn_{1-x}Fe_x)Sn$, which has been shown in Fig. S2a. Importantly, we show the optimized lattice constant (a_0) and mixing enthalpies (E_{mix}) of these alloys in Fig. 6b, where E_{mix} was found small compared to $kT_0 = 23.55$ meV (where k is the Boltzmann constant) at temperature $T_0 = 273.15$ K (0°C). Mixed alloys with a small negative mixing enthalpy ($-kT_0 < E_{mix} \leq 0$) can be uniform at ambient $T \geq T_0$. In contrast, alloys with a small positive mixing enthalpy ($0 < E_{mix} < kT_0$) can develop a compositional fluctuation, which lowers the enthalpy [14]; however, they do not segregate at $T > E_{mix}/k$. We find that $(Co_xNi_{1-x})_2MnA$ with A={Sn or Sb} have small positive E_{mix}, see Fig. 6.

$Co_2Mn(Sn_{1-x}Sb_x)$: The calculated magnetization of $Co_2Mn(Sn_{1-x}Sb_x)$ increases with x approximately linearly from 1.258 μ_B/atom in Co_2MnSn to 1.500 μ_B/atom in half-metallic Co_2MnSb. The equilibrium lattice constants are slightly smaller than those from the Hume-Rothery rule: this indicates the mixing tendency. Indeed, the trend in mixing enthalpies, calculated for the partially-ordered (KKR-CPA) and fully-ordered (VASP and KKR) systems, is the same, see Fig. 1c. The predicted stability of disordered $Co_2Mn(Sn_xSb_{1-x})$ alloys at RT agrees with the experiment [71]. The proposed compositional range of half-metals (given by n in Table 1) is confirmed by direct DFT calculations in Fig. S2a, which shows that disorder on different sublattices result into same change in n that can produce similar effects. Comparing calculations to experiment, we need to take into account that experimental samples are not always precisely stoichiometric. In particular, according to the RBS measurements [71], the Co_2MnSn sample had a an excess

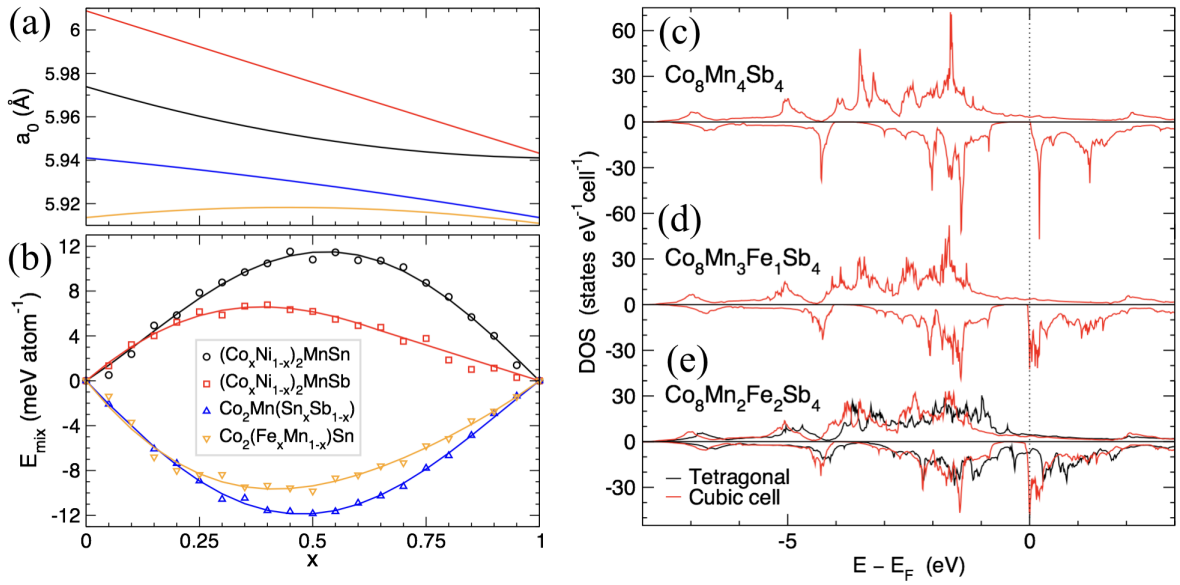

Figure 6: (a,b) The equilibrium lattice constants a_0 (Å) and mixing enthalpies E_{mix} (meV-atom^{-1}) vs. composition x for fH alloys with a homogeneous chemical disorder on one of the sublattices, obtained using KKR-CPA. Lines are the piece-wise low-degree polynomial fits to DFT data (21 points, symbols). (c-e) Total spin DOS (states/eV-f.u.) of $Co_8(Mn_{4-4x}Fe_{4x})Sb_4$ at $0 \le x \le 0.5$ for cubic Heusler (red) and tetragonal (black) 16-atom cell.

Co, i.e., $Co_{2.03}Mn_{1.00}Sn_{0.97}$, while Co_2MnSb sample was Co-deficient, i.e., $Co_{1.98}Mn_{1.01}Sb_{1.01}$ ($Co_{1.94}Mn_{1.02}Sb_{1.04}$ according to ICP). Consequently, we expect a slight difference between the equilibrium lattice constants a calculated for the ideal stoichiometric crystals at 0 K, and measured on the off-stoichiometric samples at finite T. Notably, the lattice constants from calculations and experiments [11, 71] agree within 1%, see Table S1.

($Co_{2-x}Ni_x$)MnSb: With increasing Ni concentration, magnetization is decreasing and the lattice constant is increasing (Fig. 6a). Because replacement of Co by Ni in Co_2MnSb moves E_F away from the band gap, ($Co_{2-x}Ni_x$)MnSb are not half-metals at $x > 0.03$, see Table 1.

($Co_{2-x}Ni_x$)MnSn: These alloys can be half-metallic at $0.1 < x < 0.45$, see Table 1. The rapidly quenched by melt-spinning $Ni_{47.3}Mn_{28.2}Sn_{24.5}$ sample was confirmed to be half-metallic [96]: this sample has excessive 2.7 at.%Mn replacing Ni and 0.5 at.%Mn replacing Sn. Fig. S2b shows that doping not only shifts E_F, but also narrows the band gap. Due to the peak of electronic DOS at the Fermi level (see Fig. S2b), cubic CoNiMnSn and $Co_3NiMn_2Sn_2$ structures are unstable. We find that they can be stabilized by a tetragonal distortion, and our findings agree with recent calculations [15].

$Co_2(Mn_{1-x}Fe_x)$Sn: In Co_2MnSn, the band gap in minority spins is located slightly above the Fermi level. Shifting E_F to higher energies should change this alloy into a half-metal, see Fig. S2a. Magnetization increases with x from 1.26 μ_B/atom in Co_2MnSn to 1.41 μ_B/atom in Co_2FeSn and so does the lattice constant (although the atomic radius and magnetic moment of Mn is larger than that of Fe).

$Co_2(Mn_{1-x}Fe_x)$Sb: In Co_2MnSb the E_F is located at the edge of the band gap in minority spins (Fig. 2). Replacement of Mn by Fe lowers magnetization from 1.50 μ_B in Co_2MnSb to 1.32 μ_B/atom in Co_2FeSb, while distortion of $Co_2(Mn_{0.5}Fe_{0.5})Sb$ from unstable cubic to a more stable tetragonal structure lowers magnetization from 1.42 to 1.23 μ_B/atom. An attempt to mix Mn with Fe on the Mn sublattice quickly moves E_F away from the band gap [thus, $Co_2(Mn_{1-x}Fe_x)Sb$ are not half-metals for $x > 0.0$] into the large peak in the minority spins (Fig. 6b-d), making a cubic Heusler structure unstable. Indeed, mixing enthalpies of the cubic $Co_2(Mn_{1-x}Fe_x)Sb$ structures are positive (relative to the segregated Co_2MnSb and Co_2FeSb), with that for cubic $Co_2(Mn_{0.5}Fe_{0.5})Sb$ being +2.1 meV/atom, while distorted tetragonal $Co_2(Mn_{0.5}Fe_{0.5})Sb$ has a negative formation enthalpy of −10.3 meV/atom. A similar instability towards tetragonal distortions was predicted for other Co_2-based Heusler compounds under pressure [97]. We conclude that adding iron to Co_2MnSb can result in formation of other (more stable) compounds with lower magnetization, which

are not Heusler.

4. Summary

In this work, we offer a design guide based on electron count for achieving half-metallicity in Heusler alloys, where the electron count was manipulated both by substitutional doping and disorder. The intelligent choice of alloying elements was found to tune the the total number of electrons thats shifts the Fermi-level to the band gap region, making the system half-metallic. The electronic-structure study of half-metallic compositions was performed using direct DFT methods, and found that the mixing of different alloying elements on different sublattices can produce similar effects on the electronic-structure. We also found several stable Heusler alloys their compositions, e.g., Co_2-Mn-X and Ni-Mn-X (with X={Al, Si, Ga, Ge, Sn, Sb}), with low mixing enthalpies. Based on the idea of electron count and disorder, we predicted that hH NiMnBi can be made half-metallic by substituting Ni by specific Cu and Zn compositions (($CuNi_3$)Mn_4Bi_4 and ($ZnNi_7$)Mn_8Bi_8), which also provides improved thermodynamic stability to hH NiMnBi. Our work provides prediction of numerous multicomponent half-metals with desired width of the band gap as marked in Tables 1& 2. The uniqueness of our approach lies in the fact that it provides fast electron-count based assessment of half-metallicity. The design guide presented here will play a dominant role in discovering novel compositions, which will accelerate the development and synthesis of new materials. The idea of tuning energy-gap using electron-count can also be as used a feature to train machine-learning models that will allow high-throughput design of multicomponent half-metals.

5. Acknowledgments

This work was supported by the U.S. Department of Energy (DOE), Office of Science, Basic Energy Sciences, Materials Science and Engineering Division. Application of the electronic-structure methods to caloric materials is supported by the DOE's Advanced Manufacturing Office of the Office of Energy Efficiency and Renewable Energy through CaloriCool^{TM} – the Caloric Materials Consortium, established as a part of the U.S. DOE Energy Materials Network. The research is performed at the Ames Laboratory, which is operated for the U.S. DOE by Iowa State University under contract DE-AC02-07CH11358.

6. Data availability

The authors declare that the data supporting the findings of this study are available within the paper and supplement. Also, the data that support the plots within this paper and other findings of this study are available from the corresponding author upon reasonable request.

References

[1] F. Heusler, Verh. Dtsch. Phys. Ges. 5 (1903) 219.
[2] E. Uhl, The ferromagnetic and paramagnetic properties of heusler alloys ($ni_{1-x}co_x)_2$mnsb, J. Solid State Chem. 43 (1982) 354–358.
[3] C. Felser, A. Hirohata (Eds.), Heusler Alloys: Properties, Growth, Applications, Springer, 2016.
[4] B. Weise, B. Dutta, N. Teichert, A. Hütten, T. Hickel, A. Waske, Role of disorder when upscaling magnetocaloric ni-co-mn-al heusler alloys from thin films to ribbons, Scientific Reports 8 (1) (2018) 9147. doi:10.1038/s41598-018-27428-8.
URL https://doi.org/10.1038/s41598-018-27428-8
[5] S. Li, T. Nakatani, K. Masuda, Y. Sakuraba, X. Xu, T. Sasaki, H. Tajiri, Y. Miura, T. Furubayashi, K. Hono, Enhancement of current-perpendicular-to-plane giant magnetoresistive outputs by improving b2-order in polycrystalline co2(mn0.6fe0.4)ge heusler alloy films with the insertion of amorphous cofebta underlayer, Acta Materialia 142 (2018) 49 – 57. doi:https://doi.org/10.1016/j.actamat.2017.09.046.
URL http://www.sciencedirect.com/science/article/pii/S1359645417308121
[6] M. N. Guzik, C. Echevarria-Bonet, M. D. Riktor, P. A. Carvalho, A. E. Gunnaes, M. H. Sorby, B. C. Hauback, Half-heusler phase formation and ni atom distribution in m-ni-sn (m = hf, ti, zr) systems, Acta Materialia 148 (2018) 216 – 224. doi:https://doi.org/10.1016/j.actamat.2018.01.019.
URL http://www.sciencedirect.com/science/article/pii/S1359645418300508

[7] E. Rausch, M. V. Castegnaro, F. Bernardi, M. C. M. Alves, J. Morais, B. Balke, Short and long range order of half-heusler phases in (ti,zr,hf)cosb thermoelectric compounds, Acta Materialia 115 (2016) 308 – 313. doi:https://doi.org/10.1016/j.actamat.2016.05.041.
URL http://www.sciencedirect.com/science/article/pii/S1359645416303925

[8] G. Rogl, A. Grytsiv, M. Gurth, A. Tavassoli, C. Ebner, A. Wunschek, S. Puchegger, V. Soprunyuk, W. Schranz, E. Bauer, H. Muller, M. Zehetbauer, P. Rogl, Mechanical properties of half-heusler alloys, Acta Materialia 107 (2016) 178 – 195. doi:https://doi.org/10.1016/j.actamat.2016.01.031.
URL http://www.sciencedirect.com/science/article/pii/S1359645416300301

[9] M. Gurth, G. Rogl, V. Romaka, A. Grytsiv, E. Bauer, P. Rogl, Thermoelectric high zt half-heusler alloys $ti_{1-x-y}zr_xhf_ynisn$ (0¡x¡1; 0¡y¡1), Acta Materialia 104 (2016) 210 – 222. doi:https://doi.org/10.1016/j.actamat.2015.11.022.
URL http://www.sciencedirect.com/science/article/pii/S1359645415300732

[10] J. E. Fischer, J. Karel, S. Fabbrici, P. Adler, S. Ouardi, G. H. Fecher, F. Albertini, C. Felser, Magnetic properties and curie temperatures of disordered heusler compounds: $co_{1+x}fe_{2-x}Si$, Phys. Rev. B 94 (2016) 024418. doi:10.1103/PhysRevB.94.024418.
URL https://link.aps.org/doi/10.1103/PhysRevB.94.024418

[11] K. Buschow, P. van Engen, R. Jongebreur, Magneto-optical properties of metallic ferromagnetic materials, Journal of Magnetism and Magnetic Materials 38 (1) (1983) 1 – 22. doi:http://dx.doi.org/10.1016/0304-8853(83)90097-5.
URL http://www.sciencedirect.com/science/article/pii/0304885383900975

[12] P.J. Webster, Magnetic and chemical order in heusler alloys containing cobalt and manganese, J. Phys. Chem. Solids 32 (1971) 1221–1231. doi:http://dx.doi.org/10.1016/S0022-3697(71)80180-4.

[13] P. J. Brown, K. U. Neumann, P. J. Webster, K. R. A. Ziebeck, The magnetization distributions in some heusler alloys proposed as half-metallic ferromagnets, Journal of Physics: Condensed Matter 12 (2000) 1827–1835. doi:http://stacks.iop.org/0953-8984/12/i=8/a=325.

[14] N. A. Zarkevich, D. D. Johnson, V. K. Pecharsky, High-throughput search for caloric materials: the caloricool approach, Journal of Physics D: Applied Physics 51 (2) (2018) 024002. doi:10.1088/1361-6463/aa9bd0.
URL http://stacks.iop.org/0022-3727/51/i=2/a=024002

[15] A. Grünebohm, H. C. Herper, P. Entel, On the rich magnetic phase diagram of (ni,co)-mn-sn heusler alloys, Journal of Physics D: Applied Physics 49 (39) (2016) 395001.
URL http://stacks.iop.org/0022-3727/49/i=39/a=395001

[16] R. A. de Groot, F. M. Mueller, P. G. v. Engen, K. H. J. Buschow, New class of materials: Half-metallic ferromagnets, Phys. Rev. Lett. 50 (1983) 2024–2027. doi:10.1103/PhysRevLett.50.2024.

[17] K. E. H. M. Hanssen, P. E. Mijnarends, Positron-annihilation study of the half-metallic ferromagnet nimnsb: Theory, Phys. Rev. B 34 (1986) 5009–5016. doi:10.1103/PhysRevB.34.5009.

[18] M. J. Otto, R. A. M. van Woerden, P. J. van der Valk, J. Wijngaard, C. F. van Bruggen, C. Haas, K. H. J. Buschow, Half-metallic ferromagnets. i. structure and magnetic properties of nimnsb and related inter-metallic compounds, Journal of Physics: Condensed Matter 1 (13) (1989) 2341.
URL http://stacks.iop.org/0953-8984/1/i=13/a=007

[19] S. Fujii, S. Ishida, S. Asano, Electronic structure and lattice transformation in ni2mnga and co2nbsn, Journal of the Physical Society of Japan 58 (1989) 3657–3665. doi:10.1143/JPSJ.58.3657.

[20] S. Fujii, S. Sugimura, Ishida, S. Asano, Hyperfine fields and electronic structures of the heusler alloys co 2 mnx (x=al, ga, si, ge, sn), Journal of Physics: Condensed Matter 2 (1990) 8583. doi:https://doi.org/10.1088/0953-8984/2/43/004.

[21] S. Fujii, S. Ishida, S. Asano, A half-metallic band structure and fe_2mnz (z=al, si, p), Journal of the Physical Society of Japan 64 (1995) 185–191. doi:10.1143/JPSJ.64.185.

[22] I. Galanakis, P. H. Dederichs, N. Papanikolaou, Origin and properties of the gap in the half-ferromagnetic heusler alloys, Phys. Rev. B 66 (2002) 134428. doi:10.1103/PhysRevB.66.134428.

[23] Galanakis, I. and Dederichs, P. H. and Papanikolaou, N., Slater-pauling behavior and origin of the half-metallicity of the full-heusler alloys, Phys. Rev. B 66 (2002) 174429. doi:10.1103/PhysRevB.66.174429.

[24] G.-X. Miao, J. Chang, B.A. Assaf, D. Heiman, and J. S. Moodera, Spin regulation in composite spin-filter barrier devices, Nature Comm. 5 (2014) 3682. doi:10.1038/ncomms4682.

[25] K. M. Krishnan, Fundamentals and Applications of Magnetic Materials, Oxford University Press, 2016. doi:10.1093/acprof:oso/9780199570447.001.0001.
URL http://www.oxfordscholarship.com/view/10.1093/acprof:oso/9780199570447.001.0001/acprof-9780199570447

[26] F. CAPASSO, Band-gap engineering: From physics and materials to new semiconductor devices, Science 235 (4785) (1987) 172–176. arXiv:http://science.sciencemag.org/content/235/4785/172.full.pdf, doi:10.1126/science.235.4785.172.
URL http://science.sciencemag.org/content/235/4785/172

[27] M. Schwarze, W. Tress, B. Beyer, F. Gao, R. Scholz, C. Poelking, K. Ortstein, A. A. Günther, D. Kasemann, D. Andrienko, K. Leo, Band structure engineering in organic semiconductors, Science 352 (6292) (2016) 1446–1449. arXiv:http://science.sciencemag.org/content/352/6292/1446.full.pdf, doi:10.1126/science.aaf0590.
URL http://science.sciencemag.org/content/352/6292/1446

[28] S. A. Wolf, D. D. Awschalom, R. A. Buhrman, J. M. Daughton, S. von Molnár, M. L. Roukes, A. Y. Chtchelkanova, D. M. Treger, Spintronics: A spin-based electronics vision for the future, Science 294 (2001) 1488.

[29] C. Felser and G. H. Fecher (Ed.), Spintronics: From Materials to Devices, Springer, New York, 2013. doi:10.1007/978-90-481-3832-6.

[30] D. P. Tabor, L. M. Roch, S. K. Saikin, C. Kreisbeck, D. Sheberla, J. H. Montoya, S. Dwaraknath, M. Aykol, C. Ortiz, H. Tribukait, C. Amador-Bedolla, C. J. Brabec, B. Maruyama, K. A. Persson, A. Aspuru-Guzik, Accelerating the discovery of materials for clean energy in the era of smart automation, Nature Reviews Materials 3 (5) (2018) 5–20. doi:10.1038/s41578-018-0005-z.

URL https://doi.org/10.1038/s41578-018-0005-z
[31] P. Gorai, V. Stevanović, E. S. Toberer, Computationally guided discovery of thermoelectric materials, Nature Reviews Materials 2 (2017) 17053. doi:10.1038/natrevmats.2017.53.
URL https://doi.org/10.1038/natrevmats.2017.53
[32] A. Jain, Y. Shin, K. A. Persson, Computational predictions of energy materials using density functional theory, Nature Reviews Materials 1 (2016) 15004. doi:10.1038/natrevmats.2015.4.
URL https://doi.org/10.1038/natrevmats.2015.4
[33] G. Hautier, A. Jain, S. P. Ong, From the computer to the laboratory: materials discovery and design using first-principles calculations, Journal of Materials Science 47 (21) (2012) 7317–7340. doi:10.1007/s10853-012-6424-0.
URL https://doi.org/10.1007/s10853-012-6424-0
[34] K. E. H. M. Hanssen, P. E. Mijnarends, L. P. L. M. Rabou, K. H. J. Buschow, Positron-annihilation study of the half-metallic ferromagnet nimnsb: Experiment, Phys. Rev. B 42 (1990) 1533–1540. doi:10.1103/PhysRevB.42.1533.
[35] M. P. Raphael, B. Ravel, Q. Huang, M. A. Willard, S. F. Cheng, B. N. Das, R. M. Stroud, K. M. Bussmann, J. H. Claassen, V. G. Harris, Presence of antisite disorder and its characterization in the predicted half-metal co_2MnSi, Phys. Rev. B 66 (2002) 104429. doi:10.1103/PhysRevB.66.104429.
[36] N. A. Zarkevich, Structural database for reducing cost in materials design and complexity of multiscale computations, Complexity 11 (2006) 36–42. doi:10.1002/cplx.20117.
[37] G. Kresse, J. Hafner, Ab initio molecular dynamics for liquid metals, Phys. Rev. B 47 (1993) 558–561. doi:10.1103/PhysRevB.47.558.
URL https://link.aps.org/doi/10.1103/PhysRevB.47.558
[38] G. Kresse, J. Hafner, Ab initio molecular-dynamics simulation of the liquid-metal–amorphous-semiconductor transition in germanium, Phys. Rev. B 49 (1994) 14251–14269. doi:10.1103/PhysRevB.49.14251.
URL https://link.aps.org/doi/10.1103/PhysRevB.49.14251
[39] P. E. Blöchl, Projector augmented-wave method, Phys. Rev. B 50 (1994) 17953–17979. doi:10.1103/PhysRevB.50.17953.
URL https://link.aps.org/doi/10.1103/PhysRevB.50.17953
[40] G. Kresse, D. Joubert, From ultrasoft pseudopotentials to the projector augmented-wave method, Phys. Rev. B 59 (1999) 1758–1775. doi:10.1103/PhysRevB.59.1758.
URL https://link.aps.org/doi/10.1103/PhysRevB.59.1758
[41] J. P. Perdew, A. Ruzsinszky, G. I. Csonka, O. A. Vydrov, G. E. Scuseria, L. A. Constantin, X. Zhou, K. Burke, Restoring the density-gradient expansion for exchange in solids and surfaces, Phys. Rev. Lett. 100 (2008) 136406. doi:10.1103/PhysRevLett.100.136406.
URL http://link.aps.org/doi/10.1103/PhysRevLett.100.136406
[42] H. J. Monkhorst, J. D. Pack, Special points for brillouin-zone integrations, Phys. Rev. B 13 (1976) 5188–5192. doi:10.1103/PhysRevB.13.5188.
URL https://link.aps.org/doi/10.1103/PhysRevB.13.5188
[43] P. E. Blöchl, First-principles calculations of defects in oxygen-deficient silica exposed to hydrogen, Phys. Rev. B 62 (2000) 6158–6179. doi:10.1103/PhysRevB.62.6158.
URL https://link.aps.org/doi/10.1103/PhysRevB.62.6158
[44] J. Korringa, On the calculation of the energy of a bloch wave in a metal, Physica 13 (6–7) (1947) 392–400. doi:10.1016/0031-8914(47)90013-X.
[45] W. Kohn, N. Rostoker, Solution of the schrödinger equation in periodic lattices with an application to metallic lithium, Phys. Rev. 94 (1954) 1111–1120. doi:10.1103/PhysRev.94.1111.
URL http://link.aps.org/doi/10.1103/PhysRev.94.1111
[46] D. D. Johnson, A. V. Smirnov, and S. N. Khan, MECCA: Multiple-scattering Electronic-structure Calculations for Complex Alloys. KKR-CPA Program, ver. 2.0, Iowa State University and Ames Laboratory, Ames, 2015.
[47] A. Alam, D. D. Johnson, Optimal site-centered electronic structure basis set from a displaced-center expansion: Improved results via *a priori* estimates of saddle points in the density, Phys. Rev. B 80 (2009) 125123. doi:10.1103/PhysRevB.80.125123.
URL http://link.aps.org/doi/10.1103/PhysRevB.80.125123
[48] N. E. Christensen, S. Satpathy, Pressure-induced cubic to tetragonal transition in csi, Phys. Rev. Lett. 55 (1985) 600–603. doi:10.1103/PhysRevLett.55.600.
URL http://link.aps.org/doi/10.1103/PhysRevLett.55.600
[49] A. Alam, D. D. Johnson, Structural properties and relative stability of (meta)stable ordered, partially ordered, and disordered al-li alloy phases, Phys. Rev. B 85 (2012) 144202. doi:10.1103/PhysRevB.85.144202.
URL http://link.aps.org/doi/10.1103/PhysRevB.85.144202
[50] A. Alam, S. N. Khan, A. V. Smirnov, D. M. Nicholson, D. D. Johnson, Green's function multiple-scattering theory with a truncated basis set: An augmented-kkr formalism, Phys. Rev. B 90 (2014) 205102. doi:10.1103/PhysRevB.90.205102.
URL http://link.aps.org/doi/10.1103/PhysRevB.90.205102
[51] D. D. Johnson, Modified broyden's method for accelerating convergence in self-consistent calculations, Phys. Rev. B 38 (1988) 12807–12813. doi:10.1103/PhysRevB.38.12807.
URL http://link.aps.org/doi/10.1103/PhysRevB.38.12807
[52] D. D. Johnson, D. M. Nicholson, F. J. Pinski, B. L. Gyorffy, G. M. Stocks, Density-functional theory for random alloys: Total energy within the coherent-potential approximation, Phys. Rev. Lett. 56 (1986) 2088–2091. doi:10.1103/PhysRevLett.56.2088.
URL http://link.aps.org/doi/10.1103/PhysRevLett.56.2088
[53] D. D. Johnson, F. J. Pinski, Inclusion of charge correlations in calculations of the energetics and electronic structure for random substitutional alloys, Phys. Rev. B 48 (1993) 11553–11560. doi:10.1103/PhysRevB.48.11553.
URL http://link.aps.org/doi/10.1103/PhysRevB.48.11553
[54] R. van Leeuwen, E. J. Baerends, Exchange-correlation potential with correct asymptotic behavior, Phys. Rev. A 49 (1994) 2421–2431.

doi:10.1103/PhysRevA.49.2421.
URL https://link.aps.org/doi/10.1103/PhysRevA.49.2421

[55] P. Singh, M. K. Harbola, B. Sanyal, A. Mookerjee, Accurate determination of band gaps within density functional formalism, Phys. Rev. B 87 (2013) 235110. doi:10.1103/PhysRevB.87.235110.
URL https://link.aps.org/doi/10.1103/PhysRevB.87.235110

[56] P. Singh, M. K. Harbola, and A. Mookerjee, Calculation of bandgaps in nanomaterials using Harbola-Sahni and van Leeuwen-Baerends potentials, Woodhead Publishing, Massachusetts, 2015.

[57] P. Singh, M. K. Harbola, M. Hemanadhan, A. Mookerjee, D. D. Johnson, Better band gaps with asymptotically corrected local exchange potentials, Phys. Rev. B 93 (2016) 085204. doi:10.1103/PhysRevB.93.085204.
URL http://link.aps.org/doi/10.1103/PhysRevB.93.085204

[58] P. Singh, M. K. Harbola, D. D. Johnson, Better band gaps for wide-gap semiconductors from a locally corrected exchange-correlation potential that nearly eliminates self-interaction errors, Journal of Physics: Condensed Matter 29 (42) (2017) 424001.
URL http://stacks.iop.org/0953-8984/29/i=42/a=424001

[59] B. Sadhukhan, P. Singh, A. Nayak, S. Datta, D. D. Johnson, A. Mookerjee, Band-gap tuning and optical response of two-dimensional si_xc_{1-x}: A first-principles real-space study of disordered two-dimensional materials, Phys. Rev. B 96 (2017) 054203. doi:10.1103/PhysRevB.96.054203.
URL https://link.aps.org/doi/10.1103/PhysRevB.96.054203

[60] S. Datta, P. Singh, D. Jana, C. B. Chaudhuri, M. K. Harbola, D. D. Johnson, A. Mookerjee, Exploring the role of electronic structure on photo-catalytic behavior of carbon-nitride polymorphs, Carbon 168 (2020) 125–134. doi:https://doi.org/10.1016/j.carbon.2020.04.008.
URL https://www.sciencedirect.com/science/article/pii/S0008622320303316

[61] U. van Barth, L. Hedin, A local exchange-correlation potential for the spin polarized case: I, J. Phys. C: Solid State Phys. 15 (1972) 1629–1642. doi:http://dx.doi.org/10.1088/0022-3719/5/13/012.
URL http://iopscience.iop.org/article/10.1088/0022-3719/5/13/012/pdf

[62] O. Jepsen and O. K. Andersen, The Stuttgart TB-LMTO-ASA program, version 4.7, Max-Planck-Institut für Festkörperforschung, Stuttgart, Germany, 2000.

[63] M. K. Harbola, V. Sahni, Quantum-mechanical interpretation of the exchange-correlation potential of kohn-sham density-functional theory, Phys. Rev. Lett. 62 (1989) 489–492. doi:10.1103/PhysRevLett.62.489.
URL https://link.aps.org/doi/10.1103/PhysRevLett.62.489

[64] V. Sahni and M.K. Harbola, Quantum-mechanical interpretation of the local many-body potential of density-functional theory, International Journal of Quantum Chemistry 38 (1990) 569–584. doi:10.1002/qua.560382456.
URL http://dx.doi.org/10.1002/qua.560382456

[65] M. S. M. Hemanadhan, M. K. Harbola, Testing an excited-state energy density functional and the associated potential with the ionization potential theorem, Journal of Physics B: Atomic, Molecular and Optical Physics 47 (11) (2014) 115005.
URL http://stacks.iop.org/0953-4075/47/i=11/a=115005

[66] J. P. Perdew, Generalized gradient approximation for the fermion kinetic energy as a functional of the density, Phys. Lett. A 165 (1992) 79.

[67] M. Jourdan *et al.*, Direct observation of half-metallicity in the heusler compound co2mnsi, Nat. Commun. 5 (2014) 3974. doi:10.1038/ncomms4974.

[68] J. Ma, V. I. Hegde, K. Munira, Y. Xie, S. Keshavarz, D. T. Mildebrath, C. Wolverton, A. W. Ghosh, W. H. Butler, Computational investigation of half-heusler compounds for spintronics applications, Phys. Rev. B 95 (2017) 024411. doi:10.1103/PhysRevB.95.024411.
URL https://link.aps.org/doi/10.1103/PhysRevB.95.024411

[69] N. A. Zarkevich, L.-L. Wang, and D. D. Johnson, Anomalous magneto-structural behavior of mnbi explained: A path towards an improved permanent magnet, APL Materials 2 (2014) 032103. doi:10.1063/1.4867223.

[70] S. A. Shchukarev, M. P. Morozova, and T. A. Stolyarova, Zh. Obshch. Khim. 31 (6) (1961) 1773–1777, transtaled: Russian Journal of General Chemistry **31** (6), 1657–1660 (1961).

[71] M. R. Paudel, C. S. Wolfe, H. Patton, I. Dubenko, N. Ali, J. A. Christodoulides, S. Stadler, Magnetic and transport properties of co2mnsnxsb1-x heusler alloys, Journal of Applied Physics 105 (1) (2009) 013716. doi:http://dx.doi.org/10.1063/1.3054291.
URL http://scitation.aip.org/content/aip/journal/jap/105/1/10.1063/1.3054291

[72] S. Datta, P. Singh, C. B. Chaudhuri, D. Jana, M. K. Harbola, D. D. Johnson, A. Mookerjee, Simple correction to bandgap problems in IV and III–v semiconductors: an improved, local first-principles density functional theory 31 (49) (2019) 495502. doi:10.1088/1361-648x/ab34ad.
URL https://doi.org/10.1088/1361-648x/ab34ad

[73] J. Kübler, A. R. William, C. B. Sommers, Formation and coupling of magnetic moments in heusler alloys, Phys. Rev. B 28 (1983) 1745–1755. doi:10.1103/PhysRevB.28.1745.
URL http://link.aps.org/doi/10.1103/PhysRevB.28.1745

[74] P. J. Webster, Heusler alloys, Contemporary Physics 10 (1969) 559–577. doi:10.1080/00107516908204800.

[75] S. Picozzi, A. Continenza, A. J. Freeman, co_2Mnx (x = Si, ge, sn) heusler compounds: An *ab initio* study of their structural, electronic, and magnetic properties at zero and elevated pressure, Phys. Rev. B 66 (2002) 094421. doi:10.1103/PhysRevB.66.094421.
URL http://link.aps.org/doi/10.1103/PhysRevB.66.094421

[76] C. Ciccarelli, L. Anderson, V. Tshitoyan, A. J. Ferguson, F. Gerhard, C. Gould, L. W. Molenkamp, J. Gayles, J. Zelezny, L. Smejkal, Z. Yuan, J. Sinova, F. Freimuth, T. Jungwirth, Room-temperature spin–orbit torque in nimnsb, Nature Physics 12 (2016) 855–860. doi:10.1038/NPHYS3772.

[77] L. Ritchie, G. Xiao, Y. Ji, T. Y. Chen, C. L. Chien, M. Zhang, J. Chen, Z. Liu, G. Wu, X. X. Zhang, Magnetic, structural, and transport properties of the heusler alloys co_2MnSi and nimnsb, Phys. Rev. B 68 (2003) 104430. doi:10.1103/PhysRevB.68.104430.
URL https://link.aps.org/doi/10.1103/PhysRevB.68.104430

[78] H. Allmaier, L. Chioncel, E. Arrigoni, M. I. Katsnelson, A. I. Lichtenstein, Half-metallicity in nimnsb: A variational cluster approach with ab initio parameters, Phys. Rev. B 81 (2010) 054422. doi:10.1103/PhysRevB.81.054422.
URL https://link.aps.org/doi/10.1103/PhysRevB.81.054422
[79] K. Bugayev, Y. Bychkov, Y. Konovalov, V. Kovalenko, and E. Tretyakov, Iron and Steel Production, MIR, Moscow, 1971.
[80] N. A. Zarkevich, D. D. Johnson, Coexistence pressure for a martensitic transformation from theory and experiment: Revisiting the bcc-hcp transition of iron under pressure, Phys. Rev. B 91 (17) (2015) 174104. doi:10.1103/PhysRevB.91.174104.
[81] N. A. Zarkevich, D. D. Johnson, Magneto-structural transformations via a solid-state nudged elastic band method: Application to iron under pressure, J. Chem. Phys. 143 (2015) 064707. doi:10.1063/1.4927778.
[82] P. Campbell, Permanent magnet materials and their applications, Cambridge University Press, Cambridge, New York, Melbourne, 1994.
[83] N. A. Zarkevich, D. D. Johnson, Titanium α-ω phase transformation pathway and a predicted metastable structure, Phys. Rev. B 93 (2016) 020104. doi:10.1103/PhysRevB.93.020104.
[84] N. A. Zarkevich, D. D. Johnson, Shape-memory transformations of niti: Minimum-energy pathways between austenite, martensites, and kinetically limited intermediate states, Phys. Rev. Lett. 113 (2014) 265701. doi:10.1103/PhysRevLett.113.265701.
[85] N. A. Zarkevich, D. D. Johnson, Stable atomic structure of niti austenite, Phys. Rev. B 90 (2014) 060102. doi:10.1103/PhysRevB.90.060102.
[86] N. A. Zarkevich and D. D. Johnson, Nudged-elastic band method with two climbing images: Finding transition states in complex energy landscapes, J. Chem. Phys. 142 (2) (2015) 024106. doi:http://dx.doi.org/10.1063/1.4905209.
[87] F. P. Bundy, Direct conversion of graphite to diamond in static pressure apparatus, J. Chem. Phys. 38 (3) (1963) 631. doi:10.1063/1.1733716.
[88] B. Predel, H. Ruge, Bildungsenthalpien und bindungsverhältnisse in einigen intermetallischen verbindungen vom nias-typ, Thermochimica Acta 3 (5) (1972) 411–418. doi:10.1016/0040-6031(72)87055-2.
[89] R. Villarreal, P. Singh, R. Arroyave, Metric-driven search for structurally stable inorganic compounds, Acta Materialia 202 (2021) 437–447. doi:https://doi.org/10.1016/j.actamat.2020.10.055.
URL https://www.sciencedirect.com/science/article/pii/S1359645420308533
[90] A. Togo, I. Tanaka, First principles phonon calculations in materials science, Scr. Mater. 108 (2015) 1–5.
[91] I. Galanakis, Orbital magnetism in the half-metallic heusler alloys, Phys. Rev. B 71 (2005) 012413. doi:10.1103/PhysRevB.71.012413.
URL https://link.aps.org/doi/10.1103/PhysRevB.71.012413
[92] M. Methfessel, A. T. Paxton, High-precision sampling for brillouin-zone integration in metals, Phys. Rev. B 40 (1989) 3616–3621. doi:10.1103/PhysRevB.40.3616.
URL https://link.aps.org/doi/10.1103/PhysRevB.40.3616
[93] S. Picozzi, A. Continenza, A. J. Freeman, co_2Mnx (x = Si, ge, sn) heusler compounds: An ab initio study of their structural, electronic, and magnetic properties at zero and elevated pressure, Phys. Rev. B 66 (2002) 094421. doi:10.1103/PhysRevB.66.094421.
URL https://link.aps.org/doi/10.1103/PhysRevB.66.094421
[94] P. Mavropoulos, I. Galanakis, V. Popescu, P. H. Dederichs, The influence of spin–orbit coupling on the band gap of heusler alloys 16 (48) (2004) S5759–S5762. doi:10.1088/0953-8984/16/48/043.
URL https://doi.org/10.1088/0953-8984/16/48/043
[95] S.-D. Guo, Importance of spin?orbit coupling in power factor calculations for half-heusler anib (a=ti, hf, sc, y; bsn, sb, bi), Journal of Alloys and Compounds 663 (2016) 128–133. doi:https://doi.org/10.1016/j.jallcom.2015.12.139.
URL https://www.sciencedirect.com/science/article/pii/S0925838815319307
[96] M. Nazmunnahar, T. Ryba, J. del Val, M. Ipatov, J. González, V. Hašková, P. Szabó, P. Samuely, J. Kravcak, Z. Vargova, R. Varga, Half-metallic ni2mnsn heusler alloy prepared by rapid quenching, Journal of Magnetism and Magnetic Materials 386 (Supplement C) (2015) 98 – 101. doi:https://doi.org/10.1016/j.jmmm.2015.03.066.
URL http://www.sciencedirect.com/science/article/pii/S0304885315002875
[97] M. A. Zagrebin, V. V. Sokolovskiy, V. D. Buchelnikov, Electronic and magnetic properties of the co2-based heusler compounds under pressure: first-principles and monte carlo studies, Journal of Physics D: Applied Physics 49 (35) (2016) 355004.
URL http://stacks.iop.org/0022-3727/49/i=35/a=355004
[98] N. A. Zarkevich, D. D. Johnson, Ferh ground state and martensitic transformation, Phys. Rev. B 97 (2018) 014202. doi:10.1103/PhysRevB.97.014202.
URL https://link.aps.org/doi/10.1103/PhysRevB.97.014202
[99] T. Kanomata, K. Shirakawa, T. Kaneko, Effect of hydrostatic pressure on the curie temperature of the heusler alloys ni2mnz(z = al, ga, in, sn and sb), Journal of Magnetism and Magnetic Materials 65 (1) (1987) 76 – 82. doi:http://dx.doi.org/10.1016/0304-8853(87)90312-X.
URL http://www.sciencedirect.com/science/article/pii/030488538790312X
[100] E. Uhl, The ferromagnetic and paramagnetic properties of heusler alloys (ni-co)2mnsn, Journal of Solid State Chemistry 43 (1982) 354–358.
[101] G. A. Landrum, R. Hoffmann, J. Evers, H. Boysen, The tinisi family of compounds: Structure and bonding, Inorganic Chemistry 37 (22) (1998) 5754–5763. doi:10.1021/ic980223e.
[102] Matveyeva N.M., Nikitina S.V., and Zezin S.B., Investigation of the quasi binary systems mnsn2-fesn2, mnsn2-cosn2 and fesn2-cosn2, Russ. Metall. 5 (1968) 132–134.

Supplemental Material: Effect of substitutional doping and disorder on the phase stability, magnetism, and half-metallicity of Heusler alloys

Metallic Ni_2MnX full Heusler alloys: We claim that there are no half-metals among the fH Ni_2MnX alloys. We find that the ferromagnetic Ni_2MnX fH alloys (with X from groups 13–16 and periods 3–6) are metallic, see Fig. 5. They have high magnetization (Fig. 3a); some of them are promising phases for advanced Alnico-type magnets, while several might segregate into other compounds (Fig. 4a). The electronic-structure calculations reveal a minimum with a small density of the minority spin states, located ≈ 1 eV below the Fermi level, see Fig. S1. We found that there are no half-metals among these alloys, and we do not see a practical way of transforming them into half-metals by a small amount of doping. Thus, we disagree with the suggestion that the rapidly quenched $Ni_{47.3}Mn_{28.2}Sn_{24.5}$ ribbon, prepared by melt-spinning, was half-metallic [S96]. We point that although ferromagnets can have different conductivity for two spin channels [S98], conductivity of half-metals for one of the spins is zero. We find that Ni_2MnSn is ferromagnetic, but not half-metallic. The fH Ni_2MnX alloys with X={P, As, Sb, Bi; S, Se, Te} are unstable with respect to nickel segregation (see Fig. 4a), because they have a positive formation energy relative to the segregated metallic fcc Ni and hH NiMnX.

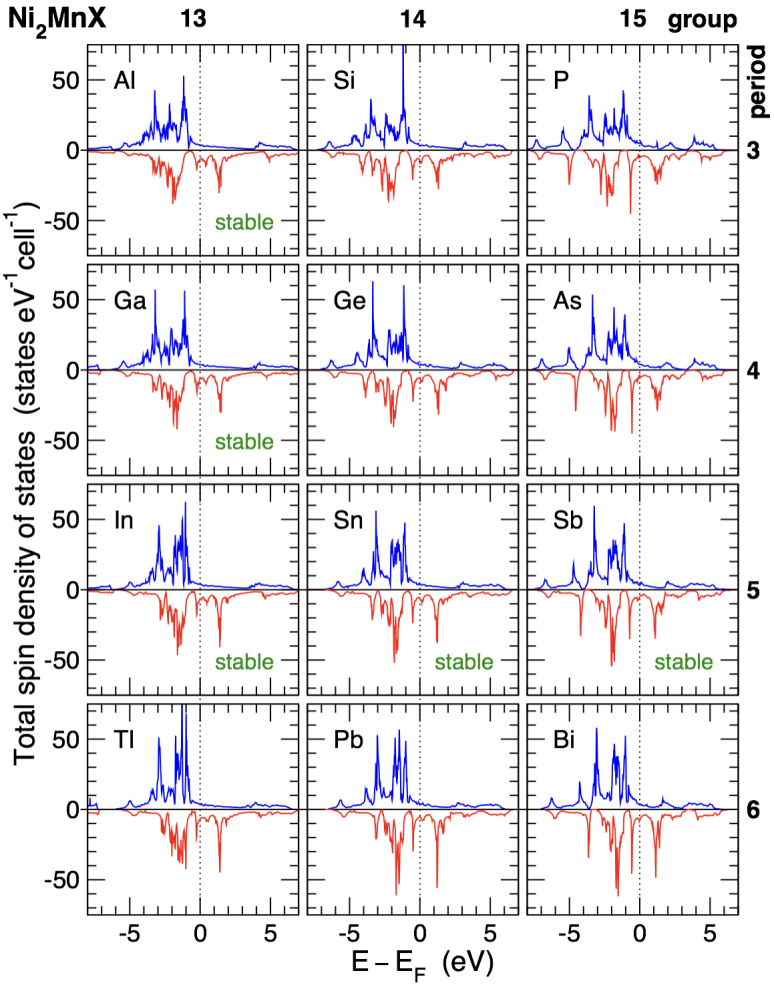

Figure S1: Total spin DOS (states/eV·f.u.) of fH Ni_2MnX alloys for 12 elements X from group 13–15 and periods 3–6). All systems are metallic. Stable compounds are known from experiment [S99, S100].

Mechanical Distortion: We considered anisotropic distortions of the cubic cells, and found that fH alloys (including

Ni_2MnSb and Ni_2MnBi) might distort along the 111 axis with energy lowering, but remain unstable with respect to segregation to fcc Ni and a hH alloy.

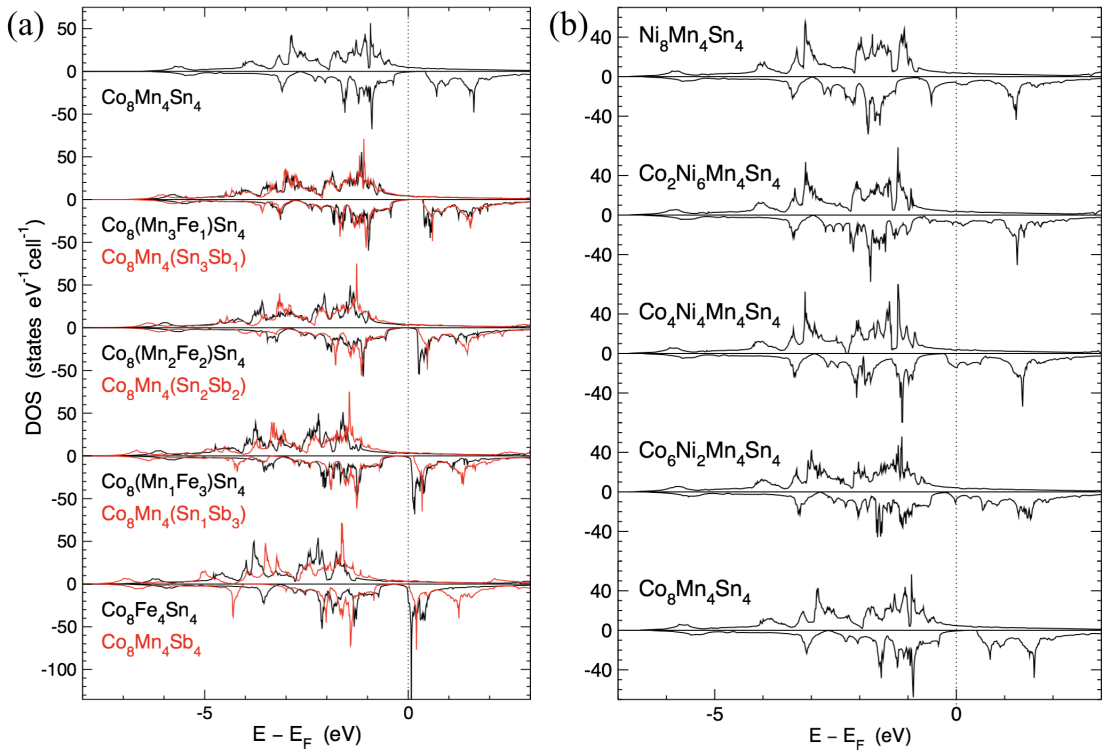

Figure S2: (Left-panel) Total spin DOS of Heusler-type $Co_8Mn_4(Sn_{4x}Sb_{4-4x})$ and $Co_8(Mn_{4-4x}Fe_{4x})Sn_4$ fully ordered cubic structures with 16 atoms per unit cell. (Right-panel) Total spin DOS (states/eV·f.u.) of $(Co_{2-x}Ni_x)MnSn$. The cubic Heusler structures with 16-atom unit cell.

Phonon calculations of NiMnBi: The phonon dispersion analysis of half-metallic NiMnBi was done using phonopy code [S90]. The phonon in Fig. S3 shows no imaginary modes, which suggests that the predicted hH compound NiMnBi is dynamically stable, which further establishes the robustness of our prediction.

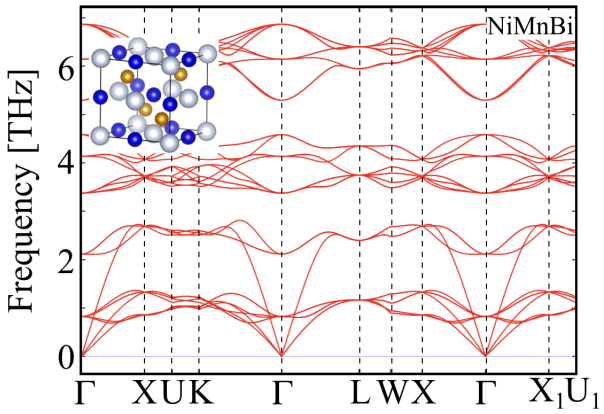

Figure S3: The phonon dispersion plot of predicted half-Heusler NiMnBi along C1b Brillouin zone (Γ-X-U-K-Γ-L-W-X-Γ-X_1-U_1) shows imaginary modes, i.e., the predicted structure is dynamically stable.

Table S1: Equilibrium lattice constant a (Å), magnetic moment M (μ_B/f.u.), and experimental [S11, S12] Curie temperature T_c (K) of fully relaxed fH Co_2MnX alloys from theory (DFT) and experiments. Asterisk (*) marks hypothetical non-existent compounds. Known competing structures include oP12 [S101] for X={Si, As} and tI12 [S102] for Co_2MnSn.

X	a(Å)		$M(\mu_B/f.u.)$		$T_c(K)$
	DFT	Expt. [S11, S12]	DFT	Expt.	Expt.
Al	5.6927	5.749[S11], 5.756[S12]	4.03	4.04, 4.01	693
Ga	5.7136	5.767[S11], 5.770[S12]	4.09	4.05, 4.05	694
In*	5.9813	–	4.44	–	–
Tl*	6.0561	–	4.80	–	–
Si	5.6285	5.645[S11], 5.654[S12]	5.00	4.90, 5.07	985
Ge	5.7358	5.749[S11], 5.743[S12]	5.00	4.93, 5.11	905
Sn	5.9854	5.984[S11], 6.000[S12]	5.03	4.79, 5.08	829
Pb*	6.0956	–	5.11	–	–
P*	5.6385	–	6.00	–	–
As*	5.7939	–	5.99	–	–
Sb	6.0182	5.943[S71]	6.00	4.52[S11]	–
Bi*	6.1793	–	6.00	–	–

Table S2: Lattice constant a (Å) of fully relaxed hH NiMnX alloys from theory (VASP–GGA) and experiment [S11, S99, S100]. Other observed competing structures are listed in the last column.

X	NiMnX GGA	hH Expt.	Other Expt.
Al	5.6078	-	
Ga	5.6182		
In	5.9521		
Tl	6.0449		
Si	5.44837		oP12 [S101]
Ge	5.570348		oP12, hP6
Sn	5.8903	-	
Pb	6.0412		
P	5.46467		oP12, hP9
As	5.637066		oP12, hP9
Sb	5.9068	5.920 [S11]	$NiMnSb_2$ hP4
Bi	6.08546		[cF88]

Table S3: Formation energies (eV/atom) of weakly stable bismuth compounds from theory and experiment.

	E (Theory) eV/atom	E (Expt.) eV/atom
MnBi	-0.102	-0.102
NiBi	-0.064	-0.020
$Ni_2Mn_5Bi_4$	-0.117	stable
$CuNi_3Mn_4Bi_4$	-0.106	—
$ZnNi_7Mn_8Bi_8$	-0.115	—